Supporting Online Material for

Electrowetting in Carbon Nanotubes

J. Y. Chen, A. Kutana, C. P. Collier,* K. P. Giapis*

*To whom correspondence should be addressed. E-mail: collier@caltech.edu (C.P.C.); giapis@cheme.caltech.edu (K.P.G.)

Published 2 December 2005, *Science* **310**, 1480 (2005)
DOI: 10.1126/science.1120385

This PDF file includes:

Materials and methods

Experimental

For SWNT probes tapping on a hard surface like HOPG, the nanotube bends or buckles elastically at higher loads and does not deflect the cantilever. The distance between the point at which the oscillation amplitude of the AFM cantilever decreases to zero and the point at which the deflection of the cantilever is detected indicates the total protrusion length of the nanotube. Once the total length is known, the immersion depth of the nanotube is determined by monitoring the amplitude damping of the oscillating cantilever as the probe contacts the mercury drop.

Probe activation also occurs routinely at positive applied voltages, as shown in Fig.S1, for a 60 nm long semiconducting carbon nanotube which is activated at +1.35V. This probe had an initial low bias resistance of 2.86±0.14 megohms, which decreases to 58.5±4.4 kilohms. After removal from the mercury surface, the resistance reverts to 2.6±0.6 megohms, consistent with the behavior seen for negative activation potentials.

A collection of additional experimental data on probe activation potentials is presented in Table S1 for various metallic and semiconducting carbon nanotube probes and their corresponding resistance values before and after activation as well as after complete removal from the mercury droplet.

Theoretical

Method

The modeling has been performed via classical molecular dynamics, by solving Newton's equations of motion for a set of atoms interacting via pairwise potentials. The details about the potentials used for mercury fluid and its interaction with the nanotube wall are provided below. The electrocapillarity effect was modeled as an external force applied to each mercury atom near the interface, as described in the paper.

Hg-Hg potential

We compared three model fluids described by Lennard-Jones (LJ) potentials and two *ab initio* Hg_2 pairwise potential for mercury dimer (S1) in terms of their ability to predict various experimental properties of mercury. Table S2 compares results for the LJ fluids with three different sets of energy well depth ε, and length scale parameter σ, as well as the original and scaled *ab initio* potentials. The first set of LJ parameters ε=750 K, σ=2.969 Å is obtained by fitting the gas-phase viscosity of mercury (S2). The second set with ε=506 K, σ=3.234 Å reproduces the binding energy and equilibrium distance of the *ab initio* mercury potential. The third set ε=378 K, σ=2.629 Å is obtained by setting the melting temperature and density of the LJ fluid equal to the experimental values for Hg. Decreasing ε leads to lowering of the melting temperature of LJ mercury, but at the same time increases the deviation of the cohesive energy and the compressibility factor from the experimental values. No choice of Lennard-Jones parameters can provide a good match for both the cohesive energy and melting temperature of Hg at the same time. On the contrary, the *ab initio* potential (S1) scaled to match the experimental density of mercury at 300 K, provides good agreement with melting temperature, while still giving the cohesive energy that is not too far from the experimental value. The scaled potential used in these simulations is of the form:

$$V(r) = \sum_{j=3}^{9} a_{2j} r^{-2j} \qquad \text{(S1)}$$

with a_6= -1.036542e+02, a_8= -1.539877e+03 a_{10}= 4.271609e+04 a_{12}= -2.975002e+05 a_{14}= 9.965436e+05 a_{16}= -1.633356e+06 a_{18}= 1.049907e+06, where the distance r is expressed in Ångstroms, and $V(r)$ is in electronvolts.

Hg-C potential

The mercury-carbon nanotube wall interaction was modeled through a pairwise Lennard-Jones potential with interaction parameters σ_{HgC} and ε_{HgC}. The length scale σ_{HgC}=3.321 Å was found by applying Lorentz-Berthelot mixing rules to the pair σ_{HgHg}=3.234 Å for the mercury dimer, and σ_{CC}=3.407 Å for graphite. The second parameter, energy ε_{HgC} was obtained from the simulation of the wetting of the graphite surface by a mercury drop.

A drop consisting of 4000 mercury atoms was put into contact with the graphite surface formed by two graphene layers with lateral dimensions of 108x107 Å, separated by 3.354 Å. Contact angles for different ε_{HgC} extracted from the shape of the droplet surface, following a procedure similar to that of de Ruijter *et al.* (S3), are plotted in Fig. S3. The linear fit of the obtained dependence yields the experimental contact angle of 152.5^{o} (*24*) at ε_{HgC}=14.7 K.

Simulation Details

The initial configuration for measuring filling speeds was achieved by immersing a nanotube into the liquid and allowing a non-wetting interface to form. The liquid was kept at 300 K during equilibration, and was disconnected from the bath at the start of electrowetting. The differences between isothermal and microcanonical runs become noticeable at voltages higher than 3 V. Results for mass transfer rates reported here are obtained from microcanonical runs. The electrocapillary pressure (ECP) was calculated by measuring an average force of interaction of a repulsive wall with the liquid mercury in the nanotube core. The repulsive wall was placed perpendicular to the nanotube axis in the middle of the 15.7 nm (20,20) carbon nanotube.

Figure captions

Figure S1. Probe current as a function of applied tip voltage for a 60 nm long semiconducting SWNT, immersed by 17±2 nm into a mercury droplet.

Figure S2. Force vs. distance curves at various applied voltages for the SWNT used to generate the data of Fig.2A. Extraction of the SWNT from the Hg droplet occurs at constant voltage, as indicated.

Figure S3. Dependence of the contact angle between mercury drop consisting of 4000 atoms and graphite surface modeled by two graphene sheets on the Hg-C interaction energy. The contact angle of 152.5^{o} is achieved at ε_{HgC}=14.7 K. The inset shows the equilibrium state of a mercury drop in contact with the graphite surface.

Figure S4. Electrowetting of a capped (20,20) SWNT by mercury: A) initial state with no potential applied shows the formation a nonwetting meniscus with the outer wall of the tube; B) 1.5 ns after application of a potential of 3.5 V, mercury rises rapidly on the outer walls of the nanotube, creating a thin wetting film.

Figure S5. Molecular dynamics simulation results for atom imbibition rates during electrocapillary filling of a (20,20) SWNT by mercury as a function of applied voltage. Note the quadratic dependence (fitting curve).

Figure S6. Electrocapillary pressure of mercury inside a (20,20) SWNT as a function of applied voltage obtained from molecular dynamics simulations. The curve represents a quadratic fit to the points.

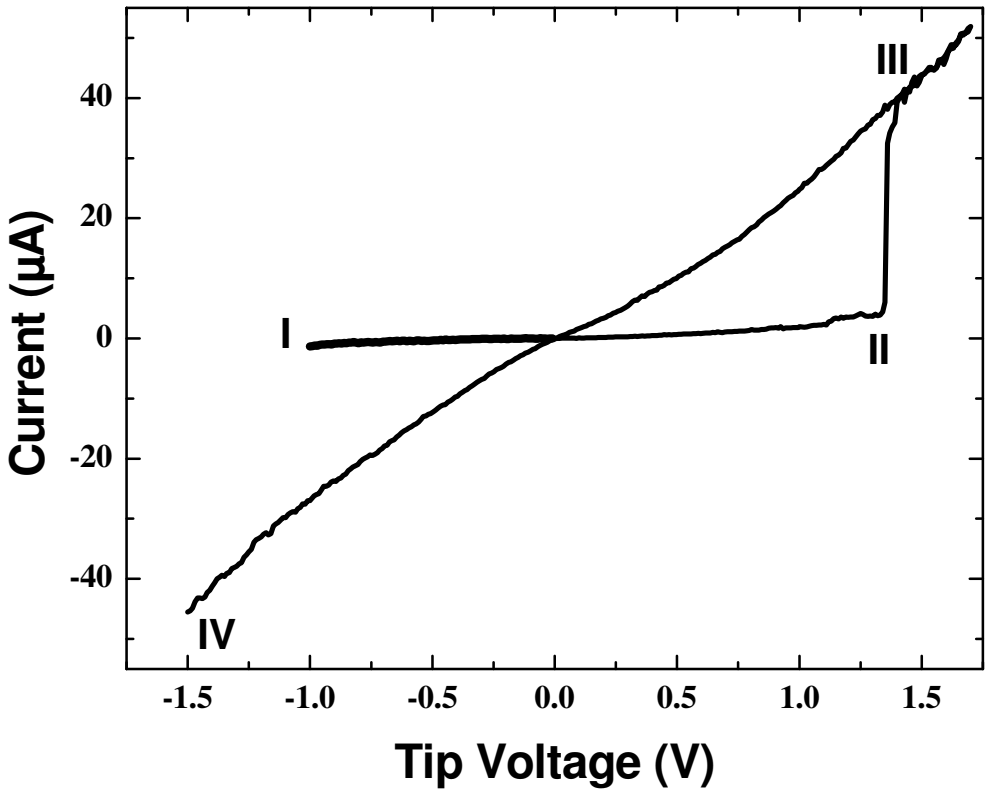

Chen *et al.*, Figure S1

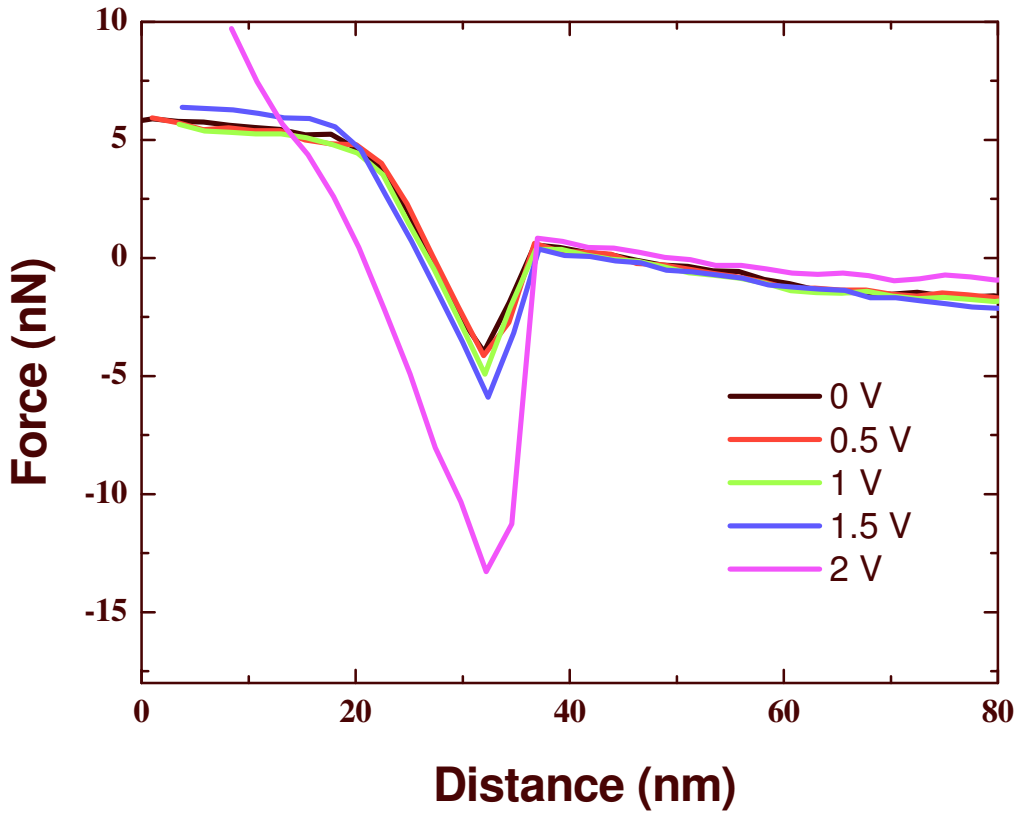

Chen *et al.*, Figure S2

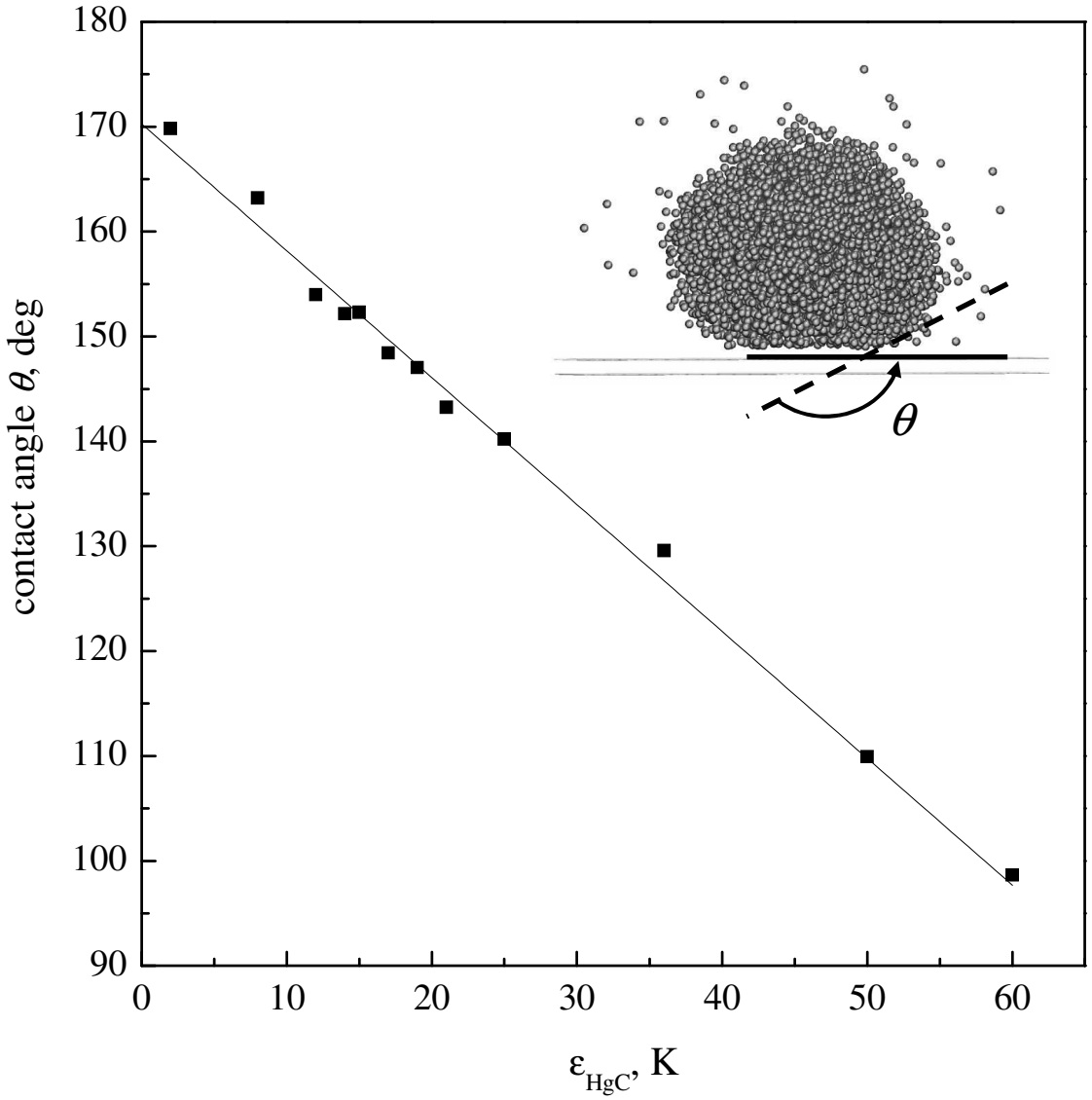

Chen *et al.*, Figure S3

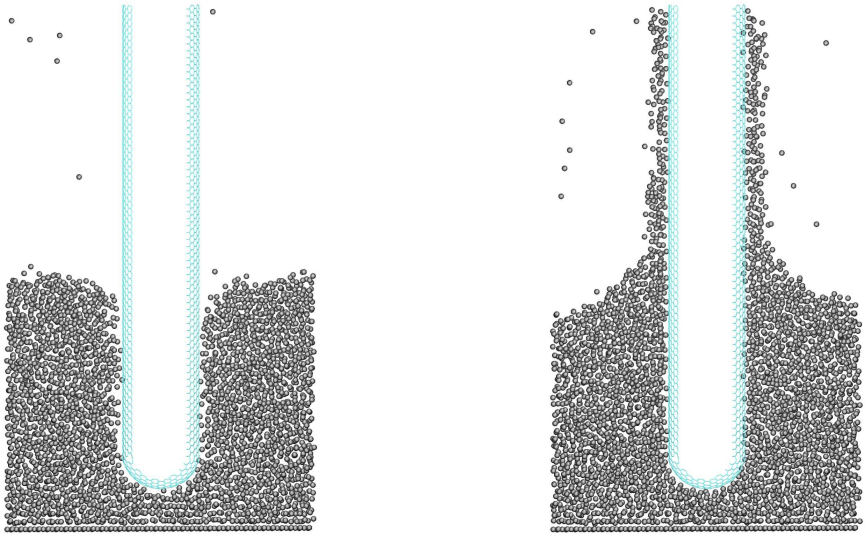

A B

Chen *et al.*, Figure S4

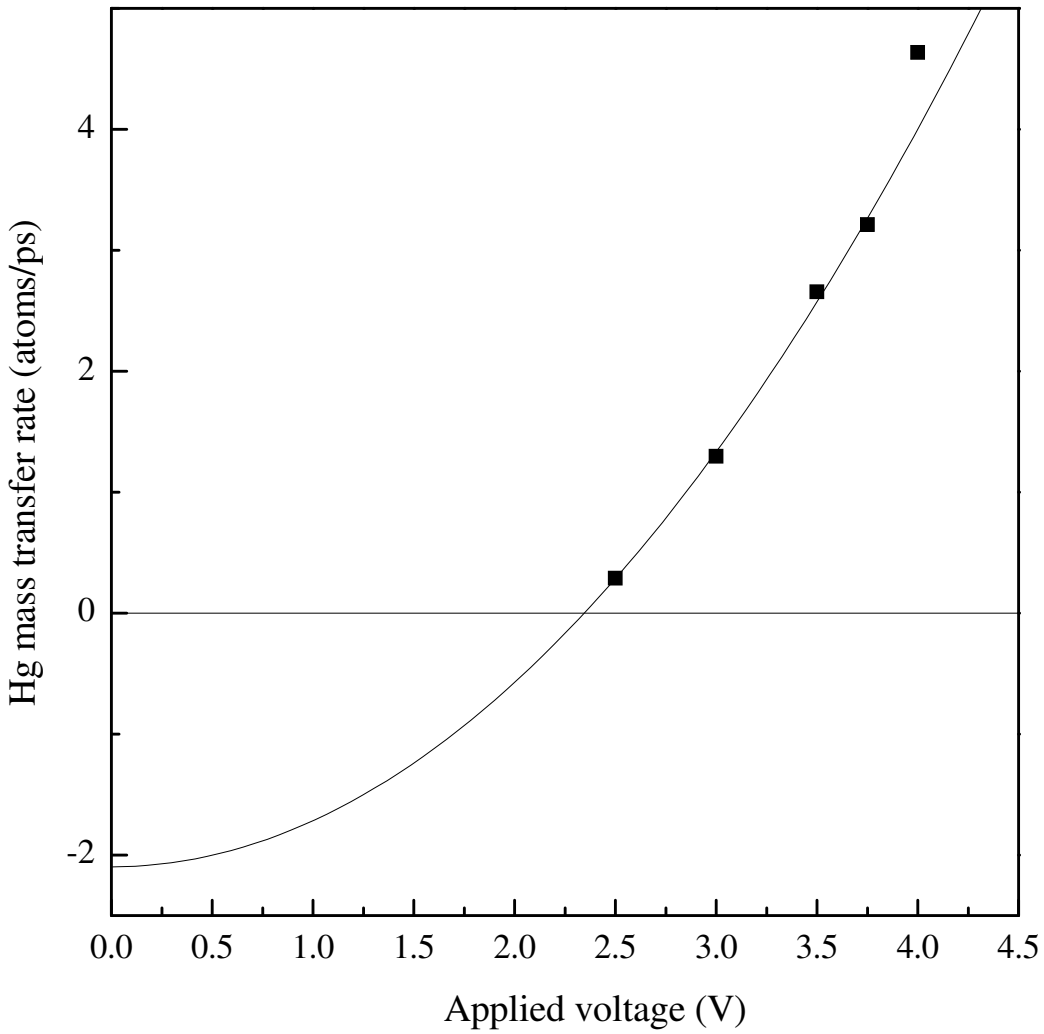

Chen *et al.*, Figure S5

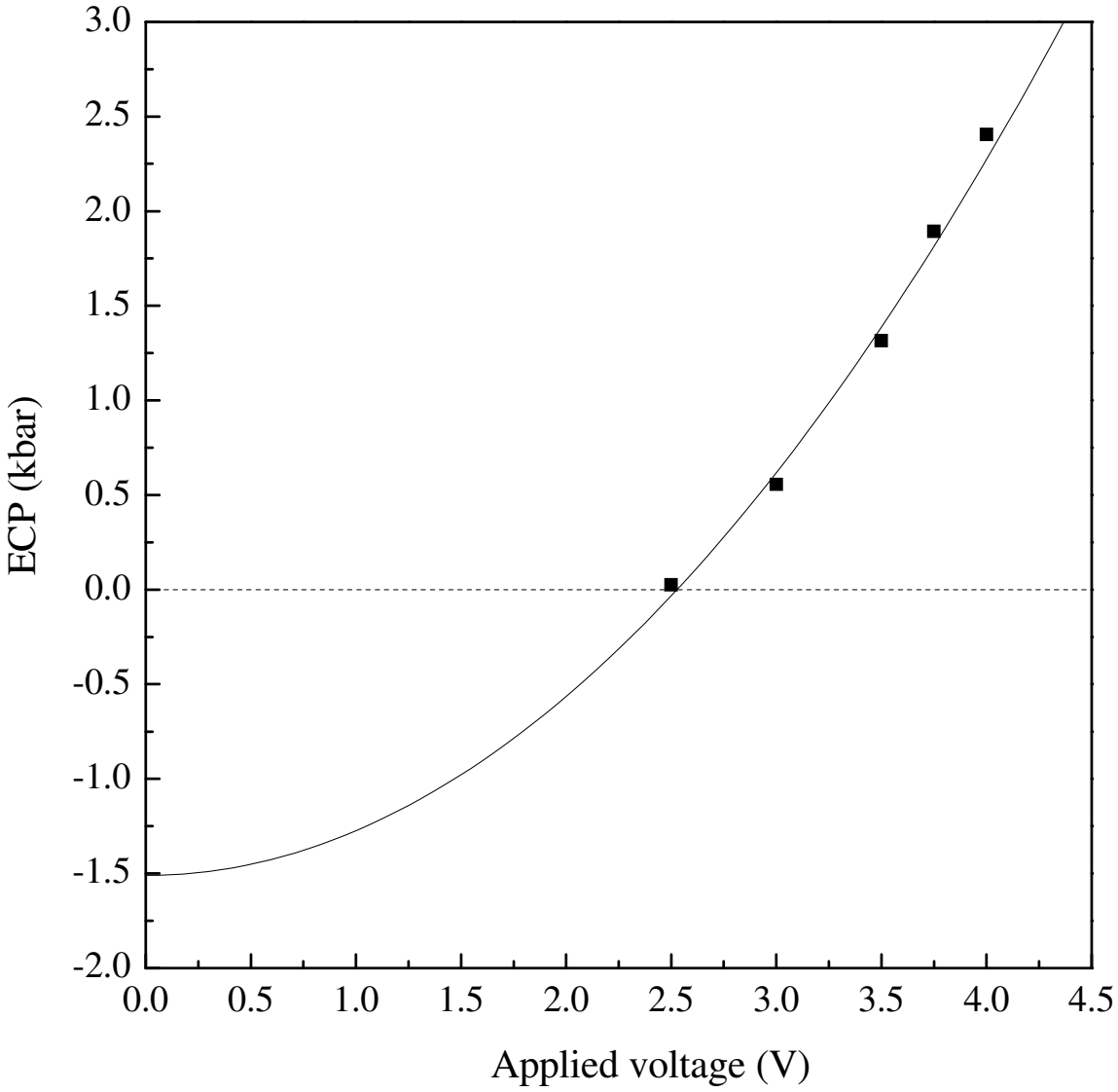

Chen *et al.*, Figure S6

Table S1. A collection of experimental data on probe activation potentials for various carbon nanotube probes and their corresponding resistance values before and after activation as well as after removal from the mercury droplet. All measurements are made at a low bias of 100 mV. N/M=not measured.

Nanotube length (nm)	Activation potential (V)	Resistance before activation	Resistance after activation	Resistance after removal
Semiconducting Nanotube				
60	1.35	2.86±0.14 MΩ	58.5 ±4.4 KΩ	2.6 ± 0.6MΩ
100	-1.26	1.16 ± 0.56MΩ	140 ±17 KΩ	Tube lost
120	-1.27	3.422±0.008 MΩ	131 ±32 KΩ	1.30±0.43 MΩ
130	-1.26	1.65 ± 0.29MΩ	46.8 ± 2.9KΩ	2.09 ± 0.76MΩ
130	-1.20	N/M	4.0 ±0.2 KΩ	Tube lost
160	1.23	843 ±64 KΩ	80 ± 14KΩ	766 ±86 KΩ
180	-1.63	6.85 ± 1.15MΩ	27.8 ±0.6 KΩ	2.8 ±0.2 MΩ
Metallic Nanotube				
45	-0.85	N/M	7.28 ±0.4 KΩ	N/M
80	-1.14	208 ±20 KΩ	29 ± 4KΩ	Tube lost
150	-1.84	289 ± 15KΩ	23.2 ± 0.6KΩ	205 ± 35KΩ
150	-0.90	174±37.2 KΩ	44.5±4.1 KΩ	96.5±13.2 KΩ
160	-2.1	170 ±34 KΩ	20.8 ± 2.1KΩ	134 ± 2KΩ
240	1.09	234 KΩ	N/M	N/M
270	N/M	102 ±3 KΩ	3.79 ± 0.18KΩ	Tube lost

Table S2 Comparison of calculated to experimental mercury properties based on different models as described in the text.

Potential	Parameters	Melting temperature T_m, K	Compress. K, $bar^{-1}x10^{-6}$	Nearest neighbor distance at 0 K R_0, Å	Cohesive energy E_{coh}, eV/atom	Density at 300 K, g/cm^3
Exper.	n/a	234	2.6[a]	2.99	0.67[b]	13.529[c]
LJ I	ε = 750.0 K σ = 2.969 Å	464	3.6	3.25	0.52	13[c]
LJ II	ε = 506.1 K σ = 3.234 Å	314	6.9	3.54	0.35	9.47[d]
LJ III	ε = 378.0 K σ = 2.629 Å	233	5.0	2.88	0.26	13.5
ab initio dimer	D_e=506.1 K r_e=3.69 Å	295	10	3.51	0.39	9.0
ab initio dimer scaled	D_e=506.1 K r_e=3.163 Å	232	8.2	2.99	0.41	13.5

[a] Ref. S4
[b] Ref. S5
[c] Ref. S6
[d] Solid at 300 K

References

S1. P. Schwerdtfeger, R. Wesendrup, and G. E. Moyano J. Chem. Phys. **115**, 7401 (2001).
S2. R. C. Reid, J. M. Prausnitz, and B. E. Poling, *The Properties of Gases and Liquids*, 4th ed. (McGraw-Hill, New York, 1987).
S3. M. J. de Ruijter, T. D. Blake, and J. De Coninck Langmuir **15**, 7836 (1999).
S4. C. Kittel, *Introduction to solid state physics*, Wiley, New York (1996).
S5. W. T. Hicks J. Chem. Phys. **38**, 1873 (1963).
S6. D. Ambrose Metrologia **27**, 245 (1990).